

Delavirdine and Dolutegravir as Potential Inhibitors of SARS-CoV-2 Main Protease (M^{pro}): An *In-Silico* Study

Fadi G. Saqallah^{1,2}, Abdulsalam Q. Almashhadani³, Belal O. Al-Najjar^{4,*} and Habibah A. Wahab^{2,3,*}

1 Discipline of Pharmaceutical Chemistry, School of Pharmaceutical Sciences, Universiti Sains Malaysia, 11800 Penang, Malaysia; *2* Pharmaceutical Design and Simulation (PhDS) Laboratory, School of Pharmaceutical Sciences, Universiti Sains Malaysia, 11800 Penang, Malaysia; *3* Discipline of Pharmaceutical Technology, School of Pharmaceutical Sciences, Universiti Sains Malaysia, 11800 Penang, Malaysia; *4* Department of Pharmaceutical Sciences, Faculty of Pharmacy, Al-Ahliyya Amman University, 19328, Amman, Jordan

Received: December 30, 2021; Revised: February 9, 2022; Accepted: February 19, 2022

Abstract

SARS-CoV-2 is a recently discovered member of coronaviruses (CoVs) family that is very contagious and has a high infectivity rate. Expanding the search for antivirals which act against SARS-CoV-2 would allow more treatment options for infected patients, accelerate their recovery time, and avoid some serious adverse effects that the limited number of approved medications might cause. In this study, we assess 74 antiviral agents, chloroquine, and hydroxychloroquine inhibitory activity against the virus's main protease (M^{pro}), which is essential for its replication. Virtual screening of the compounds has been conducted where the screened ligands were assessed according to their binding energy to the main binding pocket of M^{pro}. Ten antivirals, in addition to chloroquine and hydroxychloroquine were further studied through molecular docking simulations and assessed for their binding conformations and interactions with the protein's catalytic dyad residues. Furthermore, molecular dynamics simulations were established to study delavirdine, dolutegravir, raltegravir and vicriviroc for 100 ns. Results show that delavirdine and dolutegravir are excellent candidates that can inhibit the catalytic activity of M^{pro}. This could significantly reduce patients' hospitalisation time and the need for secondary measures.

Keywords: SARS-CoV-2, CoVID-19, main protease, delavirdine, dolutegravir

1. Introduction

Coronaviruses (CoVs) are a broad family of single-stranded RNA viruses. They can infect animals and humans, causing respiratory, gastrointestinal, hepatic, and neurological disorders (Zimmermann & Curtis, 2020). CoVs can be classified into four genera; alpha-CoV, beta-CoV, gamma-CoV, and delta-CoV, according to their protein sequences. To date, seven human coronaviruses (HCoVs) have been identified, including two alpha-CoVs; HCoV-NL63 and HCoV-229E, and five beta-CoVs; HCoV-OC43, HCoV-HKU1, the Severe Acute Respiratory Syndrome-CoV (SARS-CoV), the Middle East Respiratory Syndrome-CoV (MERS-CoV), and the Severe Acute Respiratory Syndrome-CoV-2 (SARS-CoV-2, also called CoVID-19) (Ye *et al.*, 2020; Zaki *et al.*, 2012). SARS-CoV-2 is a recently identified CoV discovered by the end of December 2019. It was identified after several Chinese health authorities observed clusters of unknown-cause pneumonia-like symptoms in Wuhan City, China (Lu *et al.*, 2020; Zhou *et al.*, 2020).

Computer-aided modelling reveals a high degree of resemblance between SARS-CoV-2 and the well-known SARS-CoV from 2002, with identical receptor-binding domain structures that maintain van der Waals forces

(Zhang *et al.*, 2020). SARS-CoV-2 recognises human ACE2 more efficiently with a stronger spike (S) protein binding affinity to human ACE2 than SARS-CoV. This increases the SARS-CoV-2 ability to spread between people (Wan *et al.*, 2020). CoVs have been identified to contain four essential proteins that can be targeted in drug discovery. These targets include spike (S), membrane (M), envelope (E), and nucleocapsid (N) proteins. However, a serine-type 3-chymotrypsin protease, also known as the main protease, 3CL^{pro} or M^{pro} (33.8 kDa), has also been identified. This enzyme is encoded by the non-structural protein 5 (NSp5). M^{pro} is an essential protein in the replication cycle of the virus. It carries out the proteolytic activity of two overlapping polyproteins; pp1a and pp1ab encoded by the replicase enzyme, and digests them into polypeptides (Fehr & Perlman, 2015; Hegyi & Ziebuhr, 2002). Today, about 353 crystal structures of SARS-CoV-2 M^{pro} are deposited in the Protein Data Bank (RCSB PDB) (Berman *et al.*, 2000). These crystal structures vary between being in their apo state or complexed with various inhibitors. A potent peptide-like irreversible inhibitor (N3P) (Figure 1) is a known inhibitor of SARS and MERS proteases which has been studied extensively for its inhibitory activity against SARS-CoV-2 M^{pro} (Jin, Du, Xu, Deng, Liu, Zhao, Zhang, Li, Zhang, Peng, *et al.*, 2020).

* Corresponding authors. e-mail: b.najjar@ammanu.edu.jo (B.O.A.-N.), habibahw@usm.my (H.A.W.).

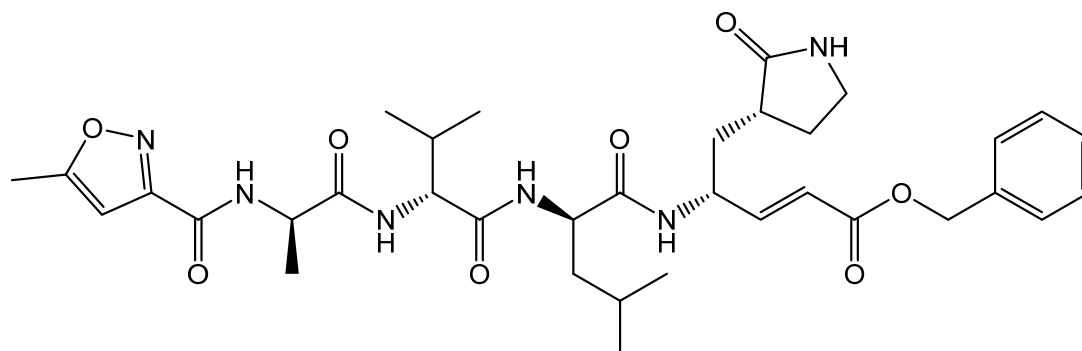


Figure 1. Irreversible peptide-like inhibitor (N3P) of coronavirus M^{pro} (sequence: 02J-ALA-VAL-LEU-PJE-010).

Patients with confirmed CoVID-19 infections show symptoms like respiratory distress, fever, cough, and shortness of breath. The incubation period seems to be between two days and up to two weeks after exposure (Carlos *et al.*, 2020). Therefore, early diagnosis of CoVID-19 is important for treating the disease and preventing it from spreading further. Many studies have found that chest computed tomography (CT) offers high sensitivity for early CoVID-19 diagnosis. However, real-time polymerase chain reaction (RT-PCR) detection of viral nucleic acid remains the reference test. Compared to RT-PCR, chest CT imaging can be a more accurate, practical, and rapid method of diagnosing and assessing the infection, especially in epidemic areas. Other diagnosis procedures of CoVID-19 include but are not limited to, clinical, physical, and laboratory diagnosis (Ai *et al.*, 2020; Zu *et al.*, 2020).

At the same time, intensive efforts by many researchers are being pushed into investigating different potential medications, including antivirals (anti-influenza and anti-HIV-1), combinations of antivirals, and anti-malaria drugs to treat SARS-CoV-2 infections. Many antiviral medications have been studied and suggested to treat SARS-CoV-2, such as lopinavir/ritonavir, ribavirin, indinavir, maraviroc, and simeprevir (Chu *et al.*, 2004; Dong *et al.*, 2020; Li & De Clercq, 2020). Recently, the US Food & Drug Administration (FDA) agency discouraged the use of these antivirals for the management of CoVID-19 infections (NIH, 2021). It is noteworthy that the use of lopinavir/ritonavir combination therapy has been found not to decrease the mortality rate or demonstrate any clinical evidence of improvement in hospitalised patients in two clinical trials (Horby, Mafham, Bell, *et al.*, 2020; Pan *et al.*, 2021). To date, the only approved antivirals for managing severe SARS-CoV-2 infections are remdesivir, Paxlovid, and molnupiravir. Remdesivir was approved in October 2020 for those above 12 years old and weighing ≥ 40 kg. Clinical trials showed a significant decrement in recovery time for patients with moderate to severe symptoms (FDA, 2020). On the other hand, Paxlovid, a trade name by Pfizer for a combination of nirmatrelvir tablets and ritonavir tablets, co-packaged for oral use, was approved recently (December 2021) by the FDA (FDA, 2021b). Paxlovid was shown to significantly decrease the need for hospitalisation and the number of deaths among severely SARS-CoV-2 infected patients (Mahase, 2021). Lastly, molnupiravir, an antiviral developed by Merck, was approved by the FDA around the same time of approving Paxlovid. Molnupiravir was announced to be

restrictively administered for patients older than 18 and at high risk for developing severe symptoms that would require hospitalisation or might lead to death (FDA, 2021a).

In this study, we focus on the potential activity of 74 antiviral agents, as well as chloroquine and hydroxychloroquine as M^{pro} inhibitors of SARS-CoV-2. This investigation aims to examine the mechanisms of binding and interactions of these antivirals, chloroquine, and hydroxychloroquine with SARS-CoV-2 M^{pro} using molecular docking, molecular dynamics, and mechanics calculations. Furthermore, exploring new antiviral agents for the management of SARS-CoV-2 infections would allow a wider choice of medications for patients with certain medical conditions which would prevent them from taking the currently approved antivirals, and for patients whom would suffer intolerable or allergic adverse reactions to the approved antivirals. The choice of M^{pro} as the target of interest comes after realising its importance in the virus life cycle and the fact that there are no correlated homologues proteins in humans.

2. Methodology

2.1. Virtual Screening

SARS-CoV-2 M^{pro} crystal structure was downloaded from Protein Data Bank (PDB) (PDB ID: 6LU7) (Berman *et al.*, 2000; Jin, Du, Xu, Deng, Liu, Zhao, Zhang, Li, Zhang, & Peng, 2020). The protease was cleaned and prepared using BIOVIA Discovery Studio 16.1 (BIOVIA, 2017). Further preparations by adding Kollman charges and polar hydrogens were done with the help of AutoDockTools 1.5.6 (Morris *et al.*, 2009) and then saved in PDBQT format (Sanner, 1999). Two-dimensional chemical structures of chloroquine, hydroxychloroquine, and the 74 antivirals were downloaded from National Institutes of Health (NIH) PubChem (Table S1, Supplementary Information) (Kim *et al.*, 2018). All compounds were compiled into one PDBQT with the help of OpenBabel 3.0.0 (O'Boyle *et al.*, 2011). Virtual screening of 500 runs among all target compounds was achieved using AutoDock Vina 1.1.2 (Trott & Olson, 2010) (Grid size: $80 \times 80 \times 80$, Coordinates: -9.732, 11.403, 68.925, as x, y, z, respectively). However, the peptide-like internal ligand (N3P) from the crystal structure of the enzyme was employed as a control inhibitor.

2.2. Molecular Docking

The top ten antivirals with the lowest binding energies determined by AutoDock Vina were selected for this step besides chloroquine, hydroxychloroquine, and the control peptide; N3P. Gasteiger charges were added. Grid and docking parameters files were prepared using AutoDockTools 1.5.6 with the same grid size and coordinates as aforementioned for 250 Genetic Algorithm runs. Docking simulations were performed using AutoDock 4.2.6 (Morris *et al.*, 2009).

2.3. Molecular Dynamics

Four antivirals with the highest affinities towards M^{pro} were selected for this part of the study. The selection of the compounds was accomplished after evaluating the docked compounds' binding energies and conformations, and the type of interactions at the binding pocket of M^{pro}, especially with the catalytic dyad residues. Molecular dynamics studies have been established with the help of AMBER 18.0 (Case *et al.*, 2018). Simulation systems were prepared by subjecting the protein crystal structure to the ff14SB forcefield and checking residues' protonation states. Ligands' topology files were prepared using Antechamber, AM1-BCC charge model, and the general AMBER force field (GAFF). Simulations were carried out in TIP3P water while adding four sodium ions to neutralise the systems. First, minimisation of the simulation systems for 10,000 steepest descent steps and 5,000 conjugate gradient steps was done. Then, gradual heating of the systems using NVT and NPT ensembles was done for 3 ns. Equilibration was further carried out for 6 ns using the NPT ensemble. Finally, a multistep production run of the systems for 100 ns was conducted using Particle Mesh Ewald Molecular Dynamics (PMEMD) engine while applying SHAKE algorithm and constant pressure periodicity (Götz *et al.*, 2012; Le Grand *et al.*, 2013; Salomon-Ferrer *et al.*, 2013). Later, MDAnalysis (Gowers *et al.*, 2019; Michaud-Agrawal *et al.*, 2011) was employed to analyse the pairwise Root Mean Square Deviation (RMSD). Further, CPPTRAJ (Roe & Cheatham III, 2013) was used to analyse the Root Mean Square Fluctuation (RMSF) of the protein, the hydrogen bonds between the binding pocket's residues and the interacting ligand, and the mass-weighted radius of gyration (RadGyr) of the non-hydrogen atoms of these residues for the last 10 ns of the simulation of each system.

2.4. Molecular Mechanics Free Energy of Binding

To calculate the free energy difference ($\Delta G_{\text{binding}}$) between the bound and unbound states of each complex, and to estimate the dynamic binding affinity, the Generalized Born Surface Area (MM-GBSA) calculations were employed (Miller III *et al.*, 2012). Energy values were calculated for the last 10,000 frames with an interval

of 100 frames, salt concentration of 0.150 M, and no quasi-harmonic entropy approximation. Runs were performed with the help of the solvated, complex, receptor, and ligand topology files.

3. Results & Discussion

3.1. Virtual Screening

Virtual screening of the 74 antivirals, chloroquine, and hydroxychloroquine against SARS-CoV-2 M^{pro} crystal structure (PDB: 6LU7) was accomplished using AutoDock Vina. The peptide-like inhibitor showed a decently low binding energy of -9.3 kcal/mol. Evaluation of the binding affinities was based on the estimated binding energies of the molecules and their binding conformations at the binding pocket. Both chloroquine and hydroxychloroquine showed low binding energies of -5.1 and -5.9 kcal/mol, respectively, suggesting that their interactions at the main pocket of M^{pro} are comparatively weak (Table 1). Moreover, their binding conformations show that the quinoline ring system of chloroquine protrudes out of the pocket groove and does not interact strongly with the surrounding amino acid residues. In contrast, hydroxychloroquine fitted nicely inside the pocket (Figure 2-a). Among the 74 antivirals, dolutegravir, maraviroc, daclatasvir, simeprevir, vicriviroc, delavirdine, lopinavir, raltegravir, indinavir, and sofosbuvir were the top antiviral molecules which bound with energy values that are very comparable to the control (≤ -8.0 kcal/mol) (Table 1). At the same time, their binding conformations occupy the active site in a way which resembles that of N3P (Figure 2-b). It should be noted that the virtual screening results are consistent with previously reported findings (Ibrahim *et al.*, 2021; Khater & Nassar, 2021). The top ten antivirals with the lowest binding energies, in addition to chloroquine and hydroxychloroquine were selected for further assessment against SARS-CoV-2 M^{pro}.

Remdesivir has been studied extensively for its inhibitory activity against M^{pro} (Daoud *et al.*, 2021; Naik *et al.*, 2020). Later studies have stated that the official target of this antiviral medication is the RNA-dependent RNA-polymerase (RdRp) (Kokic *et al.*, 2021). Nevertheless, a double-blind, randomised, placebo-controlled clinical trial was conducted to confirm the effectiveness of remdesivir, which has been found to reduce hospitalisation time and lower the chances of respiratory tract infections (Beigel *et al.*, 2020). However, another study group found that GS-441524 and its phosphorylated analogue are active metabolites of remdesivir, which act on the non-structural protein 3 (NSp3) of CoVID-19 (Ni *et al.*, 2021). These findings would explain the moderate activity of remdesivir towards M^{pro}.

Table 1. Estimated binding energies of the 74 antivirals (sorted ascendingly), chloroquine, and hydroxychloroquine in comparison with the peptide-like control (N3P) as a result of virtual screening

Compound	Binding Energy (kcal/mol)	Compound	Binding Energy (kcal/mol)
N3P (Control)	-9.3		
Chloroquine	-5.1	Cocaine	-6.7
Hydroxychloroquine	-5.9	Imiquimod	-6.7
Dolutegravir	-8.9	Valganciclovir	-6.7
Maraviroc	-8.5	Nitazoxanide	-6.6
Daclatasvir	-8.3	Telbivudine	-6.6
Simeprevir	-8.3	Edoxudine	-6.5
Vicriviroc	-8.2	Famciclovir	-6.5
Delavirdine	-8.1	Nelfinavir	-6.5
Lopinavir	-8.1	Nevirapine	-6.5
Raltegravir	-8.1	Cidofovir	-6.4
Indinavir	-8.0	Stavudine	-6.4
Sofosbuvir	-8.0	Vidarabine	-6.4
Baloxavir marboxil	-7.9	Arbidol	-6.3
Loviride	-7.9	Ganciclovir	-6.3
Podophyllotoxin	-7.9	Tenofovir	-6.3
Darunavir	-7.8	Viramidine	-6.3
Fosamprenavir	-7.8	Adefovir	-6.2
Remdesivir	-7.8	Didanosine	-6.2
Tipranavir	-7.8	Penciclovir	-6.2
Elvitegravir	-7.7	Valaciclovir	-6.2
Ritonavir	-7.7	Ribavirin	-6.1
Amprenavir	-7.6	Tromantadine	-6.0
Efavirenz	-7.6	Oseltamivir	-5.9
Pleconaril	-7.6	Peramivir	-5.9
Boceprevir	-7.5	Rimantadine	-5.9
Letermovir	-7.5	Zalcitabine	-5.9
Cobicistat	-7.4	Zanamivir	-5.9
Rilpivirine	-7.3	Ibacetabine	-5.8
Telaprevir	-7.3	Methisazone	-5.8
Doravirine	-7.2	Acyclovir	-5.7
Etravirine	-7.0	Idoxuridine	-5.7
Saquinavir	-7.0	Amantadine	-5.5
Entecavir	-6.9	Emtricitabine	-5.5
Trifluridine	-6.9	Lamivudine	-5.1
Abacavir	-6.8	Moroxydine	-5.1
Atazanavir	-6.8	Fosfonet	-4.5
Inosine	-6.8	Foscarnet	-4.3
Zidovudine	-6.8	Docosanol	-4.0

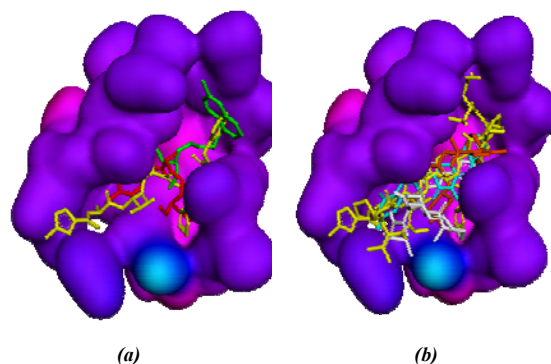


Figure 2. 3D representations of the binding conformations of the virtually screened compounds at the binding pocket of SARS-CoV-2 M^{pro}. (a) Peptide-like control (yellow), chloroquine (green), and hydroxychloroquine (red). (b) Peptide-like control (yellow), dolutegravir (light blue), maraviroc (orange), daclatasvir (light green), and simeprevir (white).

3.2. Molecular Docking

Relying on virtual screening results, molecular docking simulations of the top ten antivirals (based on their binding energies and conformations), chloroquine and hydroxychloroquine were performed using AutoDock 4.2.6. Similarly, the SARS-CoV-2 M^{pro} crystal structure (PDB: 6LU7) was chosen as a target. The crystal structure suggests that THR25, THR26, LEU27, HIS41, SER46, MET49, TYR54, PHE140, LEU141, ASN142, GLY143, CYS145, HIS163, MET165, GLU166, LEU167, PRO168, PHE185, ASP187, GLN189, THR190, ALA191, and GLN192 are the residues which build its active site. The internal bound ligand (N3P) was used as a control molecule. The lowest energies of binding and interacting amino acid residues are charted and summarised in Figure 3 and Table 2. The control inhibitor showed a quite low binding energy of -9.88 kcal/mol, which agrees with the energy value from the virtual screening. Interaction-wise, N3P was shown to interact through five hydrogen bonds with CYS145, HIS163, GLU166, GLN189, and THR190, among other various van der Waals (vdW) and Pi-interactions. It is noteworthy that N3P binds with both catalytic residues, CYS145 and HIS41, with one hydrogen bond and two Pi-sigma interactions, respectively (Table 2, Figure S1-a, Supplementary Information). The re-docked conformation of N3P was similar to its native conformation with a root mean square deviation (RMSD) of 0.92 Å (Figure 4). In comparison with the virtual screening results, chloroquine and hydroxychloroquine appeared to have higher binding affinities towards the protease; -6.96 kcal/mol, for both molecules (Table 2) which are in agreement with the previously reported values (Shivanika *et al.*, 2020; Srivastava *et al.*, 2020). Both molecules' quinoline ring systems occupy the S2 subsite at the binding pocket with a difference in their RMSDs of 0.58 Å. Chloroquine was found to interact with CYS145 and HIS41 through three Pi-interactions, whereas only one hydrogen bond can be noticed between the hydrogen atom of its secondary amine and GLN189, which can be considered as a weak interaction (Figure S1-b, Supplementary Information). In contrast, hydroxychloroquine was found to interact through four hydrogen bonds with LEU141, GLY143, SER144, and GLN189, while only interacting with the CYS145 through

a vdW interaction (Figure S1-c, Supplementary Information).

Although chloroquine and hydroxychloroquine moderately bind to M^{pro} , other studies were conducted earlier to support these findings (Mengist *et al.*, 2021; Nimgampalle *et al.*, 2020). However, it was found that other derivatives of these two ligands can *in-silico* inhibit the activity of this protein with higher affinities (Nimgampalle *et al.*, 2020). Few clinical trials were conducted to study the effectiveness of chloroquine and hydroxychloroquine in CoVID-19-infected patients. The use of hydroxychloroquine was found of no benefit in decreasing the mortality rate of hospitalised patients, in spite, its use in clinical practice increased the probability of needing to intubate in comparison to patients who received the standard of care (Horby, Mafham, Linsell, *et al.*, 2020). Another two studies found that using chloroquine with or without azithromycin was associated with prolonged QTc intervals in CoVID-19 patients (Arshad *et al.*, 2020; Nguyen *et al.*, 2020). Furthermore, Torsade de Pointes, ventricular arrhythmia, and cardiac deaths were also associated with the use of the earlier combination therapy (Nguyen *et al.*, 2020). Thus, the FDA panel discourages using chloroquine or hydroxychloroquine to treat CoVID-19 patients (NIH, 2021).

Among the docked antivirals, simeprevir, maraviroc and indinavir displayed the lowest binding energy values of -11.98, -11.82, and -10.58 kcal/mol, respectively (Table 2). Simeprevir was found to form three hydrogen bonds with HIS163, HIS164, and GLU166 while interacting with CYS145 through two aromatic Pi-sulphur bonds (Figure S1-k, Supplementary Information). Maraviroc, in contrast, was found to interact only through one hydrogen bond with GLU166 while maintaining three Pi-alkyl interactions with both catalytic residues (Figure S1-l, Supplementary Information). Still, indinavir interacted with GLU166 and GLN189 through conventional hydrogen bonds while only interacting with the catalytic residues through one vdW and one Pi-alkyl interactions (Figure S1-g, Supplementary Information). Although that vicriviroc displayed a higher binding energy (-8.22 kcal/mol) which is still comparable to that of N3P, it managed to interact using its fluorine

atoms with both CYS145 and HIS41 through hydrogen bonds. Moreover, two halogen interactions with THR26 and GLY143, and an aromatic interaction with the CYS145 residue can be noticed, suggesting a strong affinity towards the binding pocket (Table 2, Figure S1-m, Supplementary Information). Furthermore, daclatasvir, delavirdine, dolutegravir, and raltegravir displayed binding energies similar to vicriviroc (Table 2) while maintaining at least one hydrogen bond with one of the catalytic residues and several hydrophobic interactions with the other (Table 2, Figure S1-d-f and j, Supplementary Information). Finally, lopinavir and sofosbuvir were found to bind with relatively higher binding energies of -7.72 and -7.37 kcal/mol, respectively (Table 2). Interaction-wise, lopinavir did not form any hydrogen bond with the catalytic dyad, only two Pi-interactions (Figure S1-h, Supplementary Information). In contrast, sofosbuvir had five hydrogen bonds with ASN142, CYS145, HIS163, GLU166, and GLN189 and an unfavourable interaction between its sulphur atom and HIS41 (Figure S1-l, Supplementary Information). Interestingly, all the docked antiviral molecules were found to fit into the binding pocket of M^{pro} in a similar way to that of the control molecule (Figure 5), except for daclatasvir where only half of the dimeric symmetric molecule fits within the pocket, while the other half protrudes out of it towards the S4 subsite (Figure 5-c).

Based on the analyses above, only four antivirals were chosen for further investigations using molecular dynamics. Vicriviroc was chosen as it forms two hydrogen bond interactions with both residues of the catalytic dyad. Delavirdine, dolutegravir and raltegravir were chosen as they bind through one hydrogen bond with a catalytic residue while maintaining at least one hydrophobic interaction with the other. Daclatasvir was excluded as it does not fit into the active site, whereas indinavir, lopinavir, maraviroc and simeprevir could not form any hydrogen bonding with neither of the catalytic residues. Sofosbuvir was excluded from any additional assessments as it showed the highest binding energy among its peers. Similarly, chloroquine and hydroxychloroquine were disqualified from being proceeded into any further calculations.

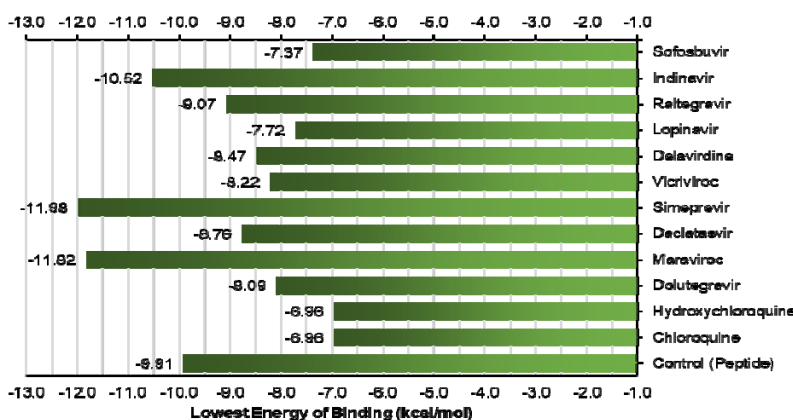


Figure 3. Histogram of the lowest binding energies (kcal/mol) of the ten antivirals, chloroquine, hydroxychloroquine, and the peptide-like control which were docked against the catalytic site of SARS-CoV-2 M^{pro} .

Table 2. The lowest energy of binding (LEB), estimated inhibition constant (K_i), and the types of interactions and their corresponding amino acids of the peptide-like inhibitor (N3P), chloroquine, hydroxychloroquine, and ten different antivirals as a result of molecular docking against SARS-CoV-2 M^{pro}.

<i>Compound</i>	<i>LEB (kcal/mol)</i>	<i>Estimated K_i</i>	<i>Hydrogen-bond Interactions</i>	<i>Pi-Interactions</i>	<i>Aromatic Interaction</i>
<i>N3P (Control)</i>	-9.91	54.10 nM	CYS145, HIS163, GLU166, GLN189, THR190	THR25, HIS41, MET49, MET165, PRO168, ALA191	THR25, PRO168, ALA191
<i>Chloroquine</i>	-6.96	7.86 uM	GLN189	HIS41, CYS145, HIS163, MET165, HIS172	HIS41, MET165, GLN189
<i>Hydroxychloroquine</i>	-6.96	7.96 uM	LEU141, GLY143, SER144, GLN189	HIS163, MET165, HIS172	MET165
<i>Daclatasvir</i>	-8.76	377.64 nM	CYS145, GLU166, PRO168, THR169, GLN189	HIS41, MET49, MET165	PRO168
<i>Delavirdine</i>	-8.47	621.04 nM	HIS41, MET165, ARG188	MET49	CYS145, MET165
<i>Dolutegravir</i>	-8.09	1.17 uM	LEU141, GLY143, SER144, CYS145, GLU166, GLN189, THR190, GLN192	LEU27, HIS41, MET165	MET165
<i>Indinavir</i>	-10.52	19.59 nM	GLU166, GLN189	HIS41, LEU141, MET165	HIS41, LEU141, MET165
<i>Lopinavir</i>	-7.72	2.21 uM	ASN142, GLN189	LEU27, HIS41, MET49, MET165, PRO168	HIS41, GLY143, MET165, PRO168
<i>Maraviroc</i>	-11.82	2.17 nM	GLU166	HIS41, MET49, CYS145, HIS163, MET165	MET165
<i>Raltegravir</i>	-9.07	225.93 nM	LEU141, CYS145, GLU166, GLN192	LEU27, MET165	MET165, PRO168
<i>Simeprevir</i>	-11.98	1.67 nM	HIS163, HIS164, GLU166	MET49, CYS145	MET49, CYS145
<i>Sofosbuvir</i>	-7.37	3.94 uM	ASN142, CYS145, HIS163, GLU166, GLN189	HIS41, MET165, GLU166	LEU27, HIS41
<i>Vicriviroc</i>	-8.22	945.16 uM	HIS41, CYS145, GLU166	LEU27, MET165, PRO168, THR190	GLY143, CYS145, THR90, ALA191

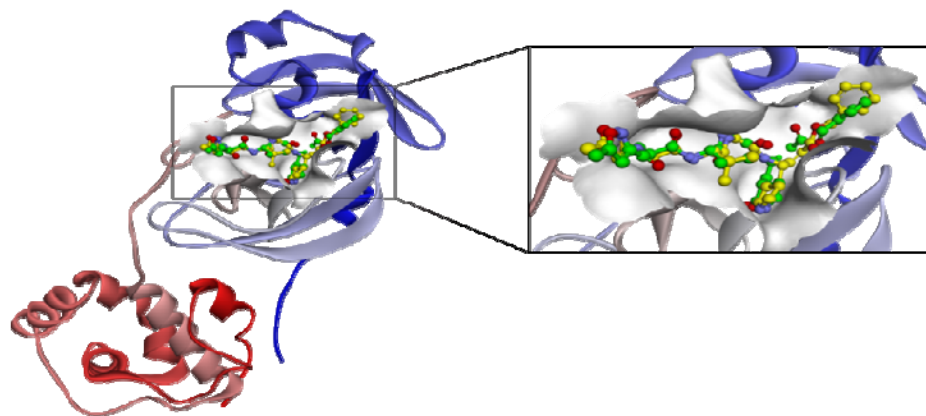


Figure 4. A 3D ribbon representation of SARS-CoV-2 M^{pro} crystal structure (PDB: 6LU7) showing the main binding pocket (white open surface) and the superimposed conformations of its internal ligand (N3P) in its native state (green) and after docking (yellow).

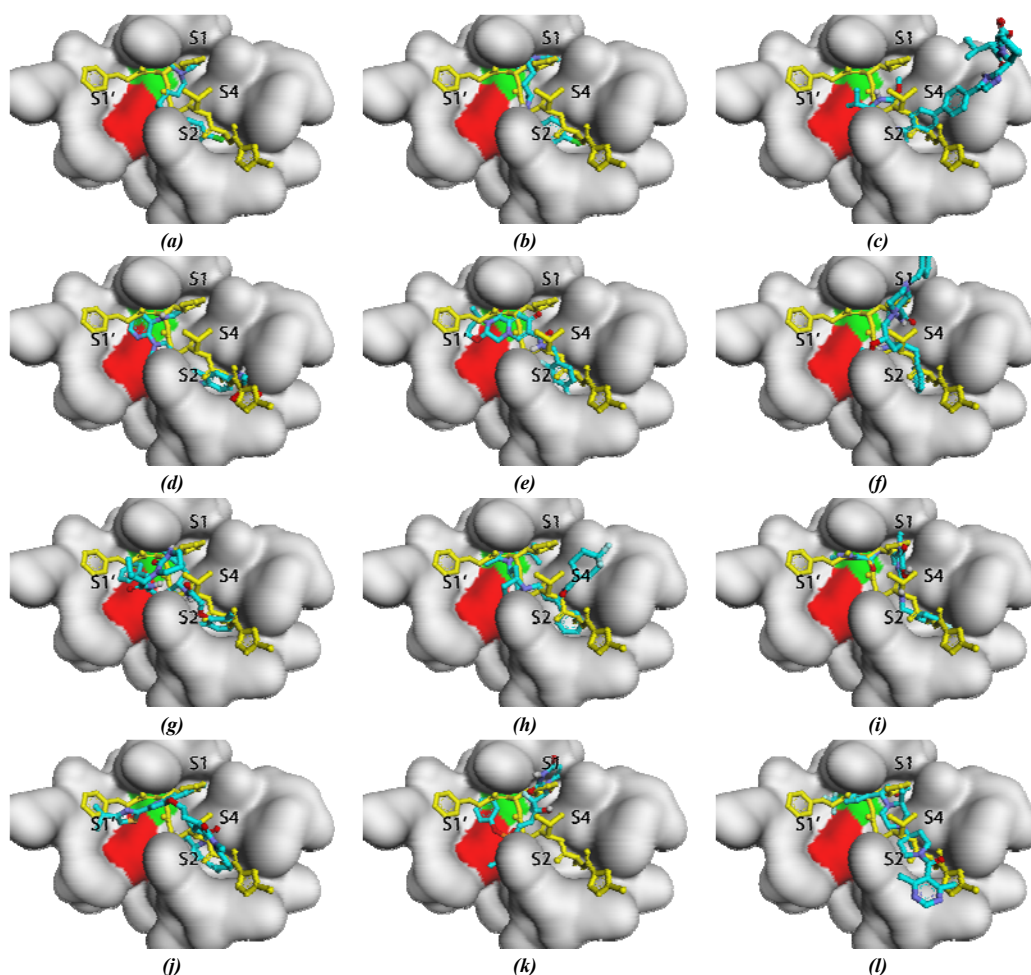


Figure 5. Binding conformations of the peptide-like control molecule (yellow), (a) chloroquine, (b) hydroxychloroquine, (c) daclatasvir, (d) delavirdine, (e) dolutegravir, (f) indinavir, (g) lopinavir, (h) maraviroc, (i) raltegravir, (j) simeprevir, (k) sofosbuvir and (l) vicriviroc at the binding pocket of SARS-CoV-2 M^{pro} (PDB: 6LU7) showing the catalytic residues; HIS41 (red) and CYS145 (green), and the subsites (S1', S1, S2, and S4).

3.3. Molecular Dynamics

Each of delavirdine, dolutegravir, raltegravir and vicriviroc, which showed the best comprehensive interactions with the catalytic residues and binding conformations from molecular docking simulations, were

employed in this part of the study, while the N3P was employed as a control inhibitor of M^{pro}.

The native form of SARS-CoV-2 M^{pro} bound to each of the four antiviral drugs was simulated through 100 ns. All four antivirals displayed a comparable resilience

interacting with the active site of the protease (Figure 6). Mean RMSD values of delavirdine-, dolutegravir-, raltegravir-, vicriviroc- and N3P-M^{pro} complexes are 2.59, 2.93, 2.38, 3.01 and 3.24 Å, respectively (Figure 7). Pairwise RMSD values of delavirdine, dolutegravir, and raltegravir are coherent and within the range of 1.0 to 3.0 Å (Figure 6-a-c). This indicates consistent stabilities of the ligand-M^{pro} complexes. Delavirdine took about 20 ns to stabilise within the binding pocket of M^{pro} (2.5-3.0 Å) (Figure 6-a), whereas it only took 10 ns for dolutegravir to achieve it (2.7-3.0 Å) (Figure 6-b). Raltegravir, on the

other hand, achieved its M^{pro}-complex stability gradually without any sharp elevation in its RMSD values (Figure 6-c). In contrast, vicriviroc's RMSD values were slightly elevated towards 4.0 Å for the most part during the first 62 ns (Figure 6-d). Whereas during the next 38 ns, it was noticed that vicriviroc leaves the main binding pocket and interacts with a distant site that is out of the scope and near the S2 and S4 subsites (data not shown). Overall, these RMSD values are significantly lower than those of the N3P-M^{pro} complex, where it was seen to elevate towards 7.5 Å, especially after 77 ns.

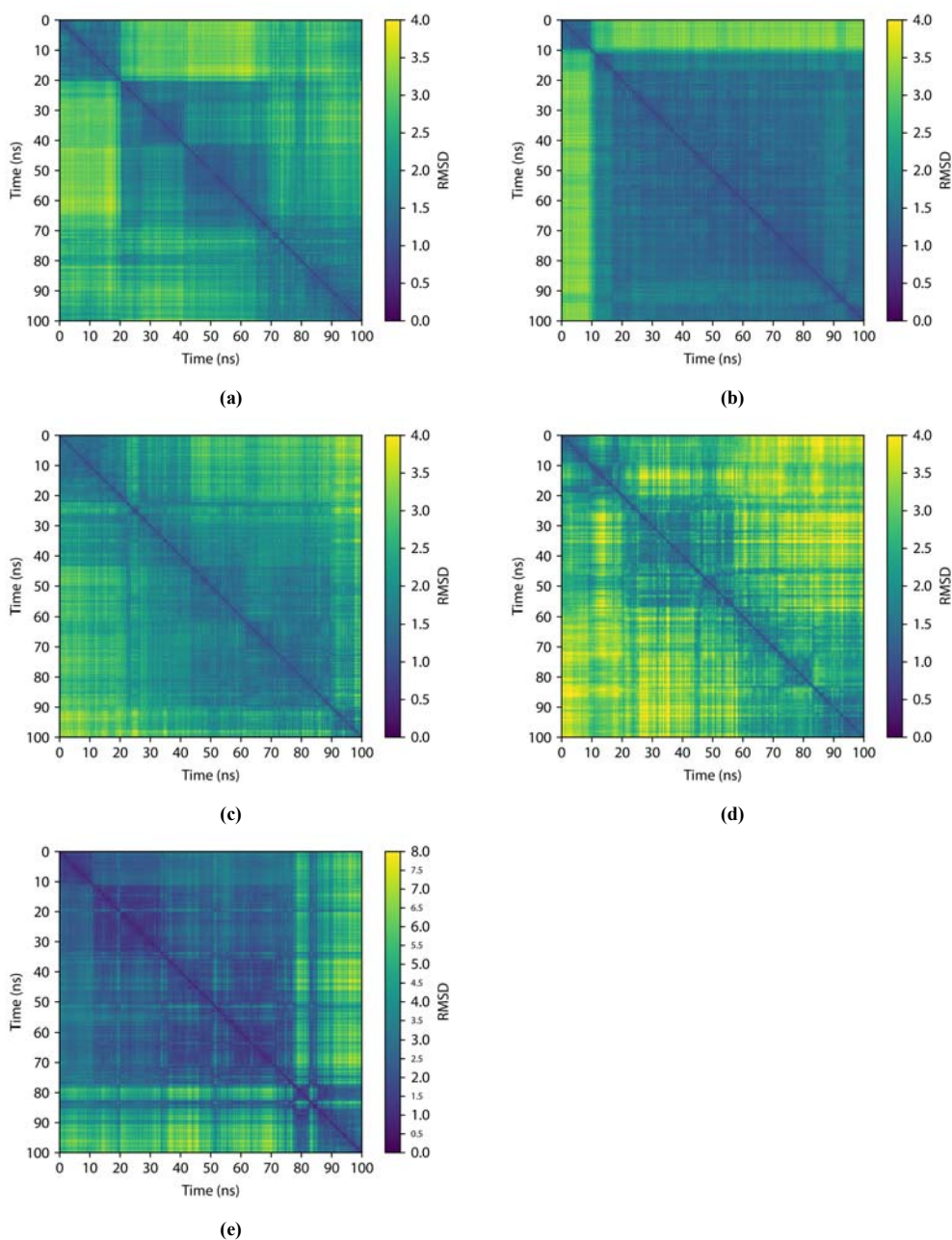


Figure 6. Heatmaps of the pairwise root mean square deviations (RMSDs) of (a) delavirdine-M^{pro}, (b) dolutegravir-M^{pro}, (c) raltegravir-M^{pro}, (d) vicriviroc-M^{pro}, and (e) N3P-M^{pro} complexes.

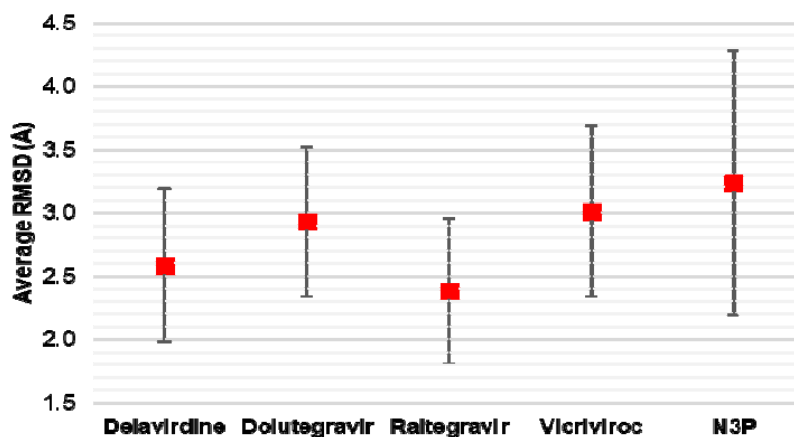


Figure 7. Average RMSD values of delavirdine-, dolutegravir-, raltegravir-, vicriviroc- and N3P-M^{pro} complexes.

The RMSF values of the ligand-M^{pro} represent fluctuated protein regions during molecular dynamics simulations. As illustrated in Figure 8, high levels of fluctuations can be noticed in the SER46, GLU47, ASP48, MET49, LEU50, ASN51, PRO52, SER139, PHE140, LEU141, ASN142 from β -turn region, ASP153, TYR154, ASP155 from the β -hairpin region, GLN189, THR190, ALA191, GLN192, ALA193 residues, and ASN274, GLY275, MET276, ASN277, GLY278, ARG279, THR280, SER301, GLY302, VAL303, THR304, PHE305,

GLN306 from β -turn region, in comparison to the rest of the amino acid residues. Each of delavirdine-, dolutegravir-, and raltegravir-M^{pro} complexes displayed similar shifts in their RMSF values. However, vicriviroc-M^{pro} showed higher and less consistent fluctuations of all residues compared to the earlier-mentioned complexes, indicating higher flexibility of the protein structure. The N3P control had the highest fluctuations, indicating that the N3P-M^{pro} complex has a more flexible nature than the other complexes.

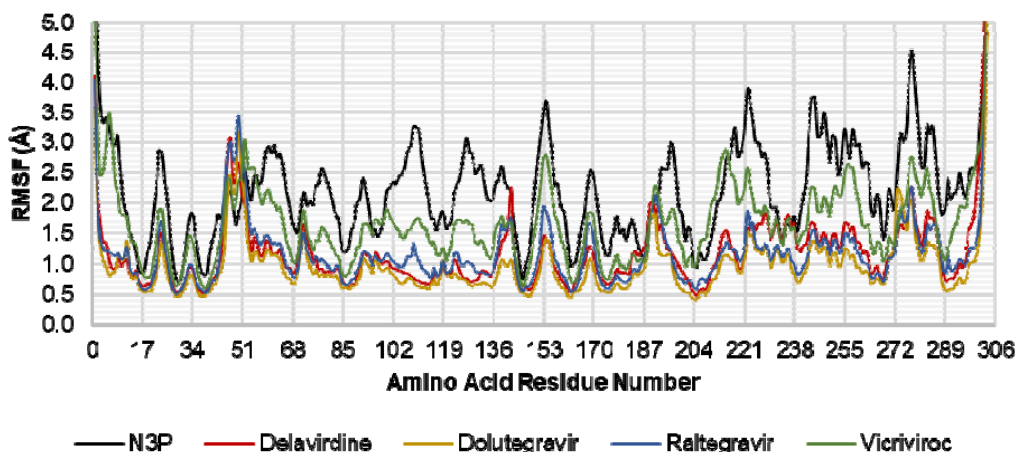


Figure 8. Root mean square fluctuations (RMSFs) of SARS-CoV-2 M^{pro} amino acid residues when in complex with delavirdine, dolutegravir, raltegravir, vicriviroc, and N3P.

Moreover, Table 3 shows the hydrogen bond analysis of protein residues and the studied ligands. In the case of delavirdine-M^{pro}, three hydrogen bonds are formed between GLU166 and the ligand for 52.23, 14.04 and 6.60% of the simulation time. Also, ASP187, ARG188 and ASN142 form hydrogen interactions with delavirdine for 26.51, 19.08 and 12.38%, respectively. Lower hydrogen bonding incidences can also be noticed with THR190 and GLN192 with shorter lifetimes. Overall, delavirdine can successfully maintain hydrogen bonding at the active site of the protease during the whole simulation time (Figure 9). Furthermore, in dolutegravir-M^{pro} complex, two hydrogen bond interactions can be seen between GLU166 and the ligand for 45.16 and 8.55%. GLY143, HIE41 and CYS145 are also residues involved in the ligand's

hydrogen bonding, with occupancies of 41.90, 20.84 and 15.12%, respectively. A lower hydrogen bond interaction lifetime is additionally seen between dolutegravir and GLN189 (Table 3). Likewise, dolutegravir can maintain hydrogen interactions with M^{pro} during the whole 100 ns of the simulation (Figure 9). In contrast, raltegravir and vicriviroc had lower overall incidences of hydrogen bonds at M^{pro} active site. Both ligands were only capable of forming two hydrogen bond interactions for each system with very short lifetimes (Table 3). Figure 9 shows a gap in the consistency of hydrogen bond interactions between raltegravir and M^{pro} (67-74 ns). This is due to the change of raltegravir's binding conformation where the *p*-fluorobenzene ring protruded outwards, while only the 2-methyloxodiazole ring occupies the binding pocket (data

not shown). Comparably, vicriviroc could not interact with the binding pocket residues after 62 ns of the simulation time. This refers to the fact that it left the main binding pocket of M^{pro} and headed towards a distant region of the protein structure, as explained earlier. In the N3P-M^{pro} complex, the ligand was found to interact with GLU166

through two hydrogen bonds with occupancies of 61.61 and 51.42%. GLN189 is another residue that is also involved through five hydrogen bond interactions of 20.88, 6.59, 5.93, 5.59 and 5.27%. Similarly, THR190 and GLY143 form hydrogen bond interactions with N3P for 13.45 and 9.69%, respectively (Table 3).

Table 3. Hydrogen bond analyses of delavirdine-, dolutegravir-, raltegravir-, vicriviroc- and N3P-M^{pro} complexes during the 100 ns molecular dynamics simulations.

<i>Complex</i>	<i>Acceptor</i>	<i>Donor H</i>	<i>Donor</i>	<i>Occupancy (%)</i>	<i>Average Distance (Å)</i>	<i>Average Angle</i>
<i>DEL-M^{pro}</i>	<i>GLU166@O</i>	<i>DEL307@H</i>	<i>DEL307@N</i>	52.23	2.82	160.83
	<i>ASP187@O</i>	<i>DEL307@H</i>	<i>DEL307@N</i>	26.51	2.85	157.11
	<i>ARG188@O</i>	<i>DEL307@H</i>	<i>DEL307@N</i>	19.08	2.84	153.71
	<i>GLU166@O</i>	<i>DEL307@H</i>	<i>DEL307@N</i>	14.04	2.83	158.33
	<i>DEL307@O</i>	<i>ASN142@H</i>	<i>ASN142@N</i>	12.38	2.85	158.09
	<i>DEL307@O</i>	<i>GLN192@H</i>	<i>GLN192@N</i>	9.88	2.88	160.38
	<i>DEL307@O</i>	<i>GLU166@H</i>	<i>GLU166@N</i>	6.60	2.89	162.50
	<i>THR190@O</i>	<i>DEL307@H</i>	<i>DEL307@N</i>	6.39	2.83	157.07
<i>DOL-M^{pro}</i>	<i>DOL307@O</i>	<i>GLU166@H</i>	<i>GLU166@N</i>	45.16	2.87	162.45
	<i>DOL307@O</i>	<i>GLY143@H</i>	<i>GLY143@N</i>	41.90	2.82	149.01
	<i>DOL307@O</i>	<i>HIE41@H</i>	<i>HIE41@N</i>	20.84	2.87	154.27
	<i>DOL307@O</i>	<i>CYS145@H</i>	<i>CYS145@N</i>	15.12	2.91	160.84
	<i>DOL307@O</i>	<i>GLU166@H</i>	<i>GLU166@N</i>	8.55	2.89	152.36
	<i>GLN189@O</i>	<i>DOL307@H</i>	<i>DOL307@N</i>	5.24	2.86	155.96
<i>RAL-M^{pro}</i>	<i>HIE164@O</i>	<i>RAL307@H</i>	<i>RAL307@N</i>	18.76	2.88	162.62
	<i>RAL307@O</i>	<i>GLN189@H</i>	<i>GLN189@N</i>	8.96	2.84	159.05
<i>VIC-M^{pro}</i>	<i>VIC307@N</i>	<i>GLN189@H</i>	<i>GLN189@N</i>	11.55	2.92	161.27
	<i>VIC307@O</i>	<i>GLU166@H</i>	<i>GLU166@N</i>	10.74	2.89	162.94
<i>N3P-M^{pro}</i>	<i>GLU166@O</i>	<i>N3P307@H</i>	<i>N3P307@N</i>	61.61	2.86	161.29
	<i>N3P307@O</i>	<i>GLU166@H</i>	<i>GLU166@N</i>	51.42	2.88	161.79
	<i>GLN189@O</i>	<i>N3P307@H</i>	<i>N3P307@N</i>	20.88	2.84	161.12
	<i>THR190@O</i>	<i>N3P307@H</i>	<i>N3P307@N</i>	13.45	2.89	154.48
	<i>N3P307@O</i>	<i>GLY143@H</i>	<i>GLY143@N</i>	9.69	2.86	155.62
	<i>GLN189@O</i>	<i>N3P307@H</i>	<i>N3P307@N</i>	6.59	2.90	163.36
	<i>N3P307@O</i>	<i>GLN189@H</i>	<i>GLN189@N</i>	5.93	2.87	159.67
	<i>N3P307@O</i>	<i>GLN189@H</i>	<i>GLN189@N</i>	5.59	2.85	159.30
	<i>N3P307@O</i>	<i>GLN189@H</i>	<i>GLN189@N</i>	5.27	2.84	161.64

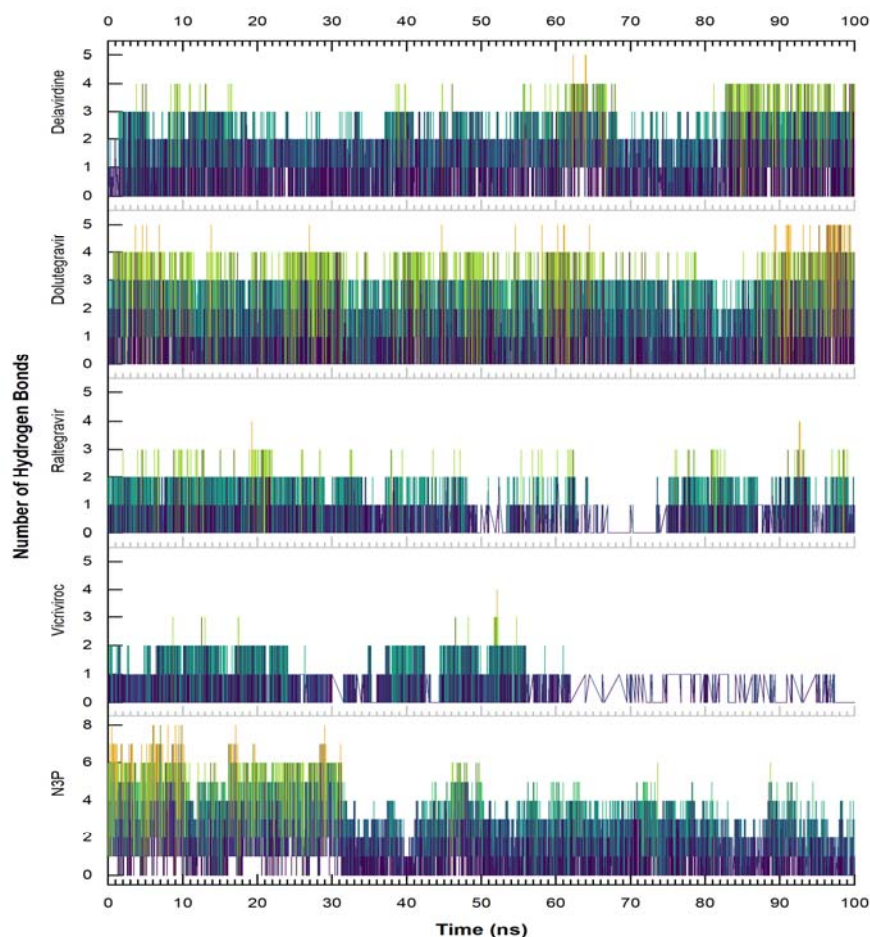


Figure 9. The frequency of hydrogen bond interactions between delavirdine, dolutegravir, raltegravir, vicriviroc and N3P within the active site of M^{pro} during the molecular dynamics simulations.

The degree of rigidity, compactness and folding of protein of the simulated systems was measured by analysing the RadGyr for the last 10 ns of the simulations time. Mean RadGyr of delavirdine-, dolutegravir-, raltegravir-, vicriviroc- and N3P- M^{pro} complexes are 11.61, 11.76, 12.39, 12.31 and 11.73 Å, respectively. It can be observed from Figure 10 that delavirdine and dolutegravir complexes with the protein have almost

similar RadGyr values and a nearly similar profile to that of N3P- M^{pro} . This indicates that the protein structure in these complexes is stable. However, the binding of raltegravir and vicriviroc to M^{pro} seems to have a higher effect on the protein compactness. RadGyr results indicate that both of the latter ligands show higher RadGyr values and fluctuations, translated into lower levels of structural rigidity.

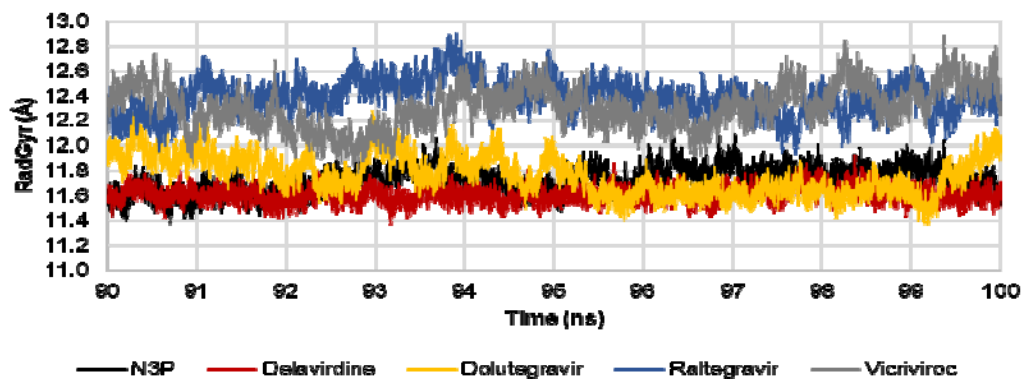


Figure 10. Time series analysis of all the simulated systems for the degree of rigidity and compactness through measuring the radius of gyrations (RadGyr) for the last 10 ns of the simulations time.

3.4. Molecular Mechanics Free Energy of Binding

MM-GBSA analyses were done for the last 10 ns of each trajectory of the simulated complexes to predict the binding free energies for the ligand-receptor. According to the energy components of the binding free energies, the major favourable contributions to the ligands binding are the van der Waals (ΔE_{vdW}) and electrostatic (ΔE_{ELE}) energies for all complexes. On the contrary, the term polar solvation-free energy (ΔE_{GB}) is largely unfavourable for binding in the five complexes. The terms ΔE_{vdW} and ΔE_{ELE} promote binding and can offset the negative effect of ΔE_{GB} . MM-GBSA values for vdW and ELE correlate with the number of hydrogen bonds. Thus, the more hydrogen bonding, the lower the ELE energy and the more favourable the vdW interactions, i.e. lower vdW energy.

Table 4. MM-GBSA binding energy analyses in kcal/mol of the last 10 ns for the simulated systems trajectories.

Complex	ΔE_{vdW}	ΔE_{ELE}	ΔE_{GB}	ΔE_{SURF}	ΔG_{gas}	ΔG_{solv}	$\Delta G_{binding}$
DEL-M ^{pro}	-37.14±2.54	-26.08±5.64	27.00±3.90	-4.42±0.31	-63.22±6.18	22.57±3.84	-40.65±3.80
DOL-M ^{pro}	-37.46±3.19	-23.90±5.86	30.07±4.07	-4.60±0.25	-61.36±6.29	25.48±3.97	-35.88±4.31
RAL-M ^{pro}	-28.93±4.73	-6.38±6.58	22.65±7.26	-3.45±0.51	-35.31±8.94	19.21±6.98	-16.11±3.84
VIC-M ^{pro}	-24.93±6.54	-3.38±4.07	10.56±4.41	-2.96±0.67	-28.31±8.65	7.60±4.00	-20.71±6.09
N3P-M ^{pro}	-49.27±3.99	-24.06±6.45	44.63±5.33	-6.12±0.55	-73.34±7.96	38.51±4.99	-34.83±4.34

ΔE_{vdW} , van der Waals contribution. ΔE_{ELE} , electrostatic contribution. ΔE_{GB} , polar solvation-free energy. ΔE_{SURF} , nonpolar solvation free energy. ΔG_{gas} , gas-phase energy; $\Delta G_{gas} = \Delta E_{vdW} + \Delta E_{ELE}$. ΔG_{solv} , total solvation free energy; $\Delta G_{solv} = \Delta E_{SURF} + \Delta E_{GB}$. $\Delta G_{binding}$, total free energy of binding; $\Delta G_{binding} = \Delta G_{gas} + \Delta G_{solv}$.

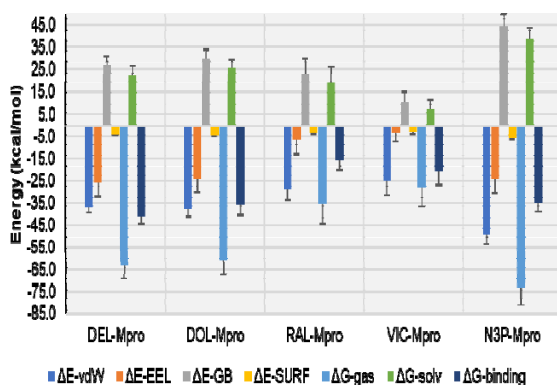


Figure 11. Histogram of the MM-GBSA binding energy analyses in kcal/mol of the last 10 ns for the simulated systems trajectories.

ΔE_{vdW} , van der Waals contribution. ΔE_{ELE} , electrostatic contribution. ΔE_{GB} , polar solvation free energy. ΔE_{SURF} , nonpolar solvation free energy. ΔG_{gas} , gas-phase energy; $\Delta G_{gas} = \Delta E_{vdW} + \Delta E_{ELE}$. ΔG_{solv} , total solvation free energy; $\Delta G_{solv} = \Delta E_{SURF} + \Delta E_{GB}$. $\Delta G_{binding}$, total free energy of binding; $\Delta G_{binding} = \Delta G_{gas} + \Delta G_{solv}$.

Overall, each of delavirdine and dolutegravir in complex with M^{pro} were found to have almost similar profiles to that of N3P, suggesting a potential inhibitory activity of the enzyme's catalytic activity, thus blocking the virus life cycle.

Delavirdine is a potent non-nucleoside reverse transcriptase inhibitor (NNRTI) of HIV-1 reverse transcriptase. It has an excellent pharmacokinetic profile and is metabolised through CYP3A4 and CYP2D6 (Tran *et al.*, 2001). On the other hand, dolutegravir is an integrase inhibitor (INI) of HIV-1 and HIV-2 integrases. Similarly, it has an excellent pharmacokinetic profile; nonetheless, it does not induce or inhibit any of the CYP

The total calculated free binding energy ($\Delta G_{binding}$) against M^{pro} for delavirdine is greater than the other antivirals and N3P (Table 4, Figure 11). Dolutegravir, however, showed a similar $\Delta G_{binding}$ to that of N3P. On the other hand, $\Delta G_{binding}$ of raltegravir and vicriviroc were significantly higher compared to the earlier mentioned ligands and the control peptide. It is noteworthy that these energy values are consistent with the hydrogen bonding analyses of the systems. Moreover, as raltegravir and vicriviroc are known to have higher water solubilities, this would explain the more favourable total solvation-free energy (ΔG_{solv}). At the same time, delavirdine and dolutegravir have much lower aqueous solubility levels, which explains how their energy values are mainly driven by vdW and ELE interactions.

isozymes (Katlama & Murphy, 2012). Both molecules showed excellent RMSD values, which are lower than that of N3P. This suggests consistent stability of delavirdine- and dolutegravir-M^{pro} complexes which the RMSF of the receptor residues can also measure. In the N3P-M^{pro} complex, it is apparent that the amino acids lining the binding pocket showed higher RMSF fluctuations signifying the flexibility of the protein in general. However, M^{pro}, when bound to either delavirdine or dolutegravir, these residues had much fewer fluctuations throughout the 100 ns of simulation time and an apparent less flexibility of the whole protein crystal structure. These findings were further supported by the degree of compactness of the systems (RadGyr). Both molecules, delavirdine and dolutegravir, had very comparable values of RadGyr to that of N3P, which indicates a sustainable degree of rigidity and protein folding. On the other hand, only delavirdine and dolutegravir managed successfully to sustain hydrogen bond interactions with the amino acid residues of the active site with occupancies and frequencies comparable to that of N3P. Moreover, molecular mechanics calculations show that both antivirals can bind through excellent binding energies, which are also comparable to N3P.

The chemical structures of delavirdine and dolutegravir provides amide bonds which resemble that of the peptide scissile bond. This would provide an excellent feature for both ligands where the catalytic dyad residues can digest this bond and in turn inhibit any further catalytic activity of the protease. However, a very limited number of studies discussed the inhibitory activity of delavirdine and dolutegravir towards SARS-CoV-2 M^{pro}. In an *in-silico* study, Al-Khafaji *et al.* suggested that delavirdine can be a potential inhibitor of the protease by binding irreversibly and covalently to its active site (Al-Khafaji *et al.*, 2021). In

contrast, a virtual screening conducted by Indu and co-workers suggested that dolutegravir can act as a potential inhibitor of M^{pro} and RdRp of CoVID-19 (Indu *et al.*, 2020). Similarly, a molecular dynamics study of both antivirals found that dolutegravir is an excellent candidate that might inhibit CoVID-19 M^{pro} by showing RMSD and RMSF fluctuations that agree with our findings. However, in the same study, although delavirdine was found to have a similar RMSD profile to our results, it caused higher shifts and fluctuations of the protein RMSF and a lower binding energy than that of dolutegravir (Sharma & Deep, 2020).

4. Conclusion

In conclusion, our results validate the ability of the N3P peptide-like molecule to irreversibly inhibit SARS-CoV-2 M^{pro} despite it having some major fluctuations in its RMSF values. Comparably, chloroquine and hydroxychloroquine do not provide a good enough inhibitory activity towards the protease, although the FDA panel now does not recommend the use of both medications for CoVID-19 infections. Among the 74 antivirals, remdesivir; an FDA-approved antiviral for controlling CoVID-19 infections, was confirmed not to act by inhibiting M^{pro}. In spite, it acts as an RdRp inhibitor. Therefore, only delavirdine and dolutegravir are proposed as excellent inhibitors of M^{pro}. However, more investigations are required to confirm and validate the inhibitory activity of these two antivirals towards M^{pro} through *in-vitro*, *in-vivo* and clinical studies. This would provide a wider range of options to treat and control CoVID-19 infections in patients by minimising hospitalisation and recovery time and probably eliminate the need for ventilators, intubation, and oxygen supplies.

Acknowledgement

This research was supported by USM RU TOP-DOWN for the project titled Catalogue of USM-RIKEN Natural Product (CURINaP) Library for the Discovery of Bioactive molecules on Ageing and Ageing Related Diseases (1001/PFARMASI/870031).

Data Availability

Data that support this study are available in the article and accompanying the supplementary material provided after the References section.

References

Ai, T., Yang, Z., Hou, H., *et al.* 2020. Correlation of chest CT and RT-PCR testing in coronavirus disease 2019 (COVID-19) in China: a report of 1014 cases. *Radiology*, **296**(2): 200642.

Al-Khafaji, K., Al-Duhaidahawi, D., & Taskin Tok, T. 2021. Using integrated computational approaches to identify safe and rapid treatment for SARS-CoV-2. *J Biomol Struct Dyn*, **39**(9): 3387-3395.

Arshad, S., Kilgore, P., Chaudhry, Z. S., *et al.* 2020. Treatment with hydroxychloroquine, azithromycin, and combination in patients hospitalized with COVID-19. *Int J Infect Dis*, **97**: 396-403.

Beigel, J. H., Tomashek, K. M., Dodd, L. E., *et al.* 2020. Remdesivir for the Treatment of Covid-19 — Final Report. *N Engl J Med*, **383**(19): 1813-1826.

Berman, H. M., Westbrook, J., Feng, Z., *et al.* 2000. The Protein Data Bank. *Nucleic Acids Res*, **28**(1): 235-242.

BIOVIA. 2017. Discovery Studio Modeling Environment, *San Diego*.

Carlos, W. G., Dela Cruz, C. S., Cao, B., *et al.* 2020. Novel wuhan (2019-nCoV) coronavirus. *Am J Respir Crit Care Med*, **201**(4): 7-8.

Case, D. A., Ben-Shalom, I. Y., Brozell, S. R., *et al.* 2018. AMBER 2018. *University of California, San Francisco*.

Chu, C. M., Cheng, V. C. C., Hung, I. F. N., *et al.* 2004. Role of lopinavir/ritonavir in the treatment of SARS: initial virological and clinical findings. *Thorax*, **59**(3): 252-256.

Daoud, S., Alabed, S. J., & Dahabiyeh, L. A. 2021. Identification of potential COVID-19 main protease inhibitors using structure-based pharmacophore approach, molecular docking and repurposing studies. *Acta Pharm*, **71**(2): 163-174.

Dong, L., Hu, S., & Gao, J. 2020. Discovering drugs to treat coronavirus disease 2019 (COVID-19). *Drug Discov Ther*, **14**(1): 58-60.

FDA. 2020. FDA Approves First Treatment for COVID-19. *US Food & Drug Administration* Retrieved 08-02-2022 from <https://www.fda.gov/news-events/press-announcements/fda-approves-first-treatment-covid-19>

FDA. 2021a. Coronavirus (COVID-19) Update: FDA Authorizes Additional Oral Antiviral for Treatment of COVID-19 in Certain Adults. *US Food & Drug Administration* Retrieved 08-02-2022 from <https://www.fda.gov/news-events/press-announcements/coronavirus-covid-19-update-fda-authorizes-additional-oral-antiviral-treatment-covid-19-certain>

FDA. 2021b. Coronavirus (COVID-19) Update: FDA Authorizes First Oral Antiviral for Treatment of COVID-19. *US Food & Drug Administration* Retrieved 08-02-2022 from <https://www.fda.gov/news-events/press-announcements/coronavirus-covid-19-update-fda-authorizes-first-oral-antiviral-treatment-covid-19>

Fehr, A. R., & Perlman, S. 2015. Coronaviruses: an overview of their replication and pathogenesis. *Methods in molecular biology (Clifton, NJ)*, **1282**: 1-23.

Götz, A. W., Williamson, M. J., Xu, D., *et al.* 2012. Routine microsecond molecular dynamics simulations with AMBER on GPUs. 1. Generalized born. *J Chem Theory Comput*, **8**(5): 1542-1555.

Gowers, R. J., Linke, M., Barnoud, J., *et al.* 2019. MDAnalysis: a Python package for the rapid analysis of molecular dynamics simulations. *Proc of the 15th Python in Science Conf*: 98-105.

Hegyí, A., & Ziebuhr, J. 2002. Conservation of substrate specificities among coronavirus main proteases. *J Gen Virol*, **83**(3): 595-599.

Horby, P. W., Mafham, M., Bell, J. L., *et al.* 2020. Lopinavir-ritonavir in patients admitted to hospital with COVID-19 (RECOVERY): a randomised, controlled, open-label, platform trial. *Lancet*, **396**(10259): 1345-1352.

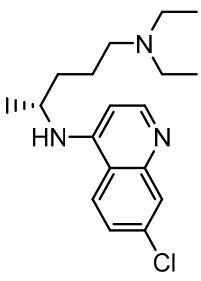
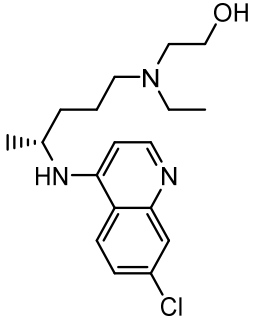
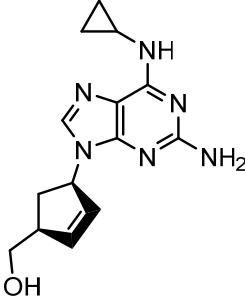
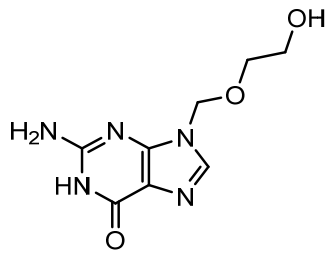
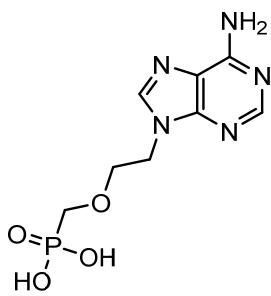
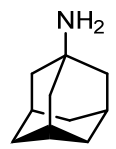
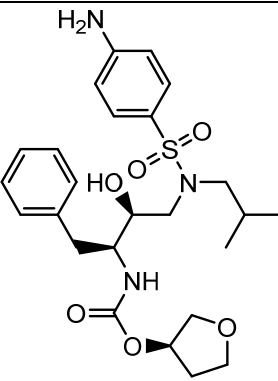
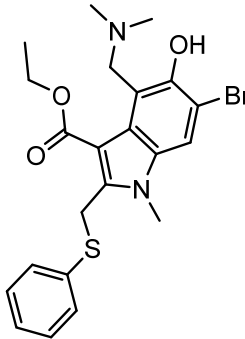
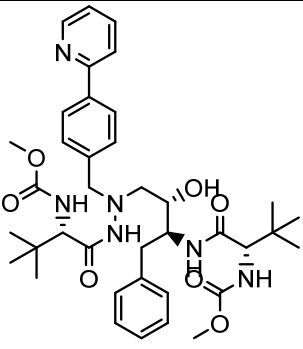
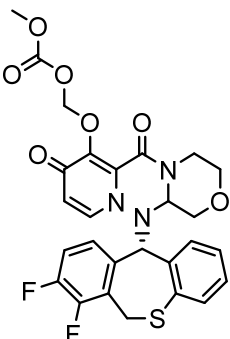
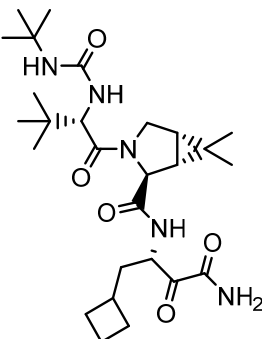
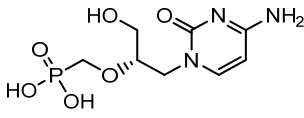
Horby, P. W., Mafham, M., Linsell, L., *et al.* 2020. Effect of Hydroxychloroquine in Hospitalized Patients with Covid-19. *N Engl J Med*, **383**(21): 2030-2040.

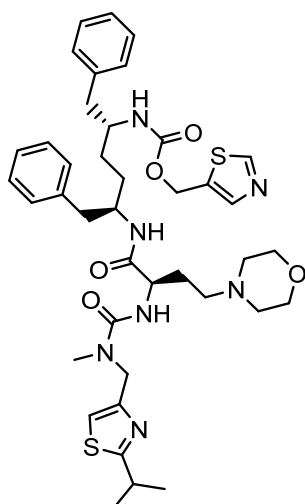
Ibrahim, M. A. A., Abdelrahman, A. H. M., Allemailem, K. S., *et al.* 2021. In silico evaluation of prospective anti-COVID-19 drug candidates as potential SARS-CoV-2 main protease inhibitors. *The Protein Journal*, **40**(3): 296-309.

- Indu, P., Rameshkumar, M. R., Arunagirinathan, N., et al. 2020. Raltegravir, Indinavir, Tipranavir, Dolutegravir, and Etravirine against main protease and RNA-dependent RNA polymerase of SARS-CoV-2: A molecular docking and drug repurposing approach. *J Infect Public Health*, **13**(12): 1856-1861.
- Jin, Z., Du, X., Xu, Y., et al. 2020. Structure of Mpro from COVID-19 virus and discovery of its inhibitors. *Nature*, **582**: 289-293.
- Katlama, C., & Murphy, R. 2012. Dolutegravir for the treatment of HIV. *Expert Opin Investig Drugs*, **21**(4): 523-530.
- Khater, I., & Nassar, A. 2021. In silico molecular docking analysis for repurposed antiviral drugs against SARS-CoV-2 main protease. *Biochem Biophys Res*, **27**: 101032.
- Kim, S., Chen, J., Cheng, T., et al. 2018. PubChem 2019 update: improved access to chemical data. *Nucleic Acids Res*, **47**(D1): 1102-1109.
- Kocic, G., Hillen, H. S., Tegunov, D., et al. 2021. Mechanism of SARS-CoV-2 polymerase stalling by remdesivir. *Nat Commun*, **12**(1): 1-7.
- Le Grand, S., Götz, A. W., & Walker, R. C. 2013. SPFP: Speed without compromise—A mixed precision model for GPU accelerated molecular dynamics simulations. *Comput Phys Commun*, **184**(2): 374-380.
- Li, G., & De Clercq, E. 2020. Therapeutic options for the 2019 novel coronavirus (2019-nCoV). *Nat Rev Drug Discov*, **19**: 149-150.
- Lu, H., Stratton, C. W., & Tang, Y. W. 2020. Outbreak of Pneumonia of Unknown Etiology in Wuhan China: the Mystery and the Miracle. *J Med Virol*, **94**(4): 401-402.
- Mahase, E. 2021. Covid-19: Pfizer's paxlovid is 89% effective in patients at risk of serious illness, company reports. *BMJ*, **375**: 2713.
- Mengist, H. M., Dilnessa, T., & Jin, T. 2021. Structural basis of potential inhibitors targeting SARS-CoV-2 main protease. *Front Chem*, **9**: 622898.
- Michaud-Agrawal, N., Denning, E. J., Woolf, T. B., et al. 2011. MDAnalysis: a toolkit for the analysis of molecular dynamics simulations. *J Comput Chem*, **32**(10): 2319-2327.
- Miller III, B. R., McGee Jr, T. D., Swails, J. M., et al. 2012. MMPBSA.py: an efficient program for end-state free energy calculations. *J Chem Theory Comput*, **8**(9): 3314-3321.
- Morris, G. M., Huey, R., Lindstrom, W., et al. 2009. AutoDock4 and AutoDockTools4: Automated docking with selective receptor flexibility. *J Comput Chem*, **30**(16): 2785-2791.
- Naik, V. R., Munikumar, M., Ramakrishna, U., et al. 2020. Remdesivir (GS-5734) as a therapeutic option of 2019-nCoV main protease - in silico approach. *J Biomol Struct Dyn*, **39**(13): 4701-4714.
- Nguyen, L. S., Dolladille, C., Drici, M.-D., et al. 2020. Cardiovascular toxicities associated with hydroxychloroquine and azithromycin: an analysis of the World Health Organization Pharmacovigilance Database. *Circulation*, **142**(3): 303-305.
- Ni, X., Schröder, M., Olieric, V., et al. 2021. Structural Insights into Plasticity and Discovery of Remdesivir Metabolite GS-441524 Binding in SARS-CoV-2 Macrodomein. *ACS Med Chem Lett*, **12**(4): 603-609.
- NIH. 2021. COVID-19 Treatment Guidelines: Antiviral Drugs That Are Approved or Under Evaluation for the Treatment of COVID-19. *National Institutes of Health*. Retrieved 29-06-2021 from <https://www.covid19treatmentguidelines.nih.gov/therapies/antiviral-therapy/>
- Ningampalle, M., Devanathan, V., & Saxena, A. 2020. Screening of Chloroquine, Hydroxychloroquine and its derivatives for their binding affinity to multiple SARS-CoV-2 protein drug targets. *J Biomol Struct Dyn*, **39**(14): 4949-4961.
- O'Boyle, N. M., Banck, M., James, C. A., et al. 2011. Open Babel: An open chemical toolbox. *J Cheminform*, **3**(1): 33.
- Pan, H., Peto, R., Henao-Restrepo, A. M., et al. 2021. Repurposed Antiviral Drugs for Covid-19 - Interim WHO Solidarity Trial Results. *N Engl J Med*, **384**(6): 497-511.
- Roe, D. R., & Cheatham III, T. E. 2013. PTRAJ and CPPTRAJ: software for processing and analysis of molecular dynamics trajectory data. *J Chem Theory Comput*, **9**(7): 3084-3095.
- Salomon-Ferrer, R., Götz, A. W., Poole, D., et al. 2013. Routine microsecond molecular dynamics simulations with AMBER on GPUs. 2. Explicit solvent particle mesh Ewald. *J Chem Theory Comput*, **9**(9): 3878-3888.
- Sanner, M. F. 1999. Python: a programming language for software integration and development. *J Mol Graph Model*, **17**(1): 57-61.
- Sharma, S., & Deep, S. 2020. In-silico drug repurposing for targeting SARS-CoV-2 main protease (M^{pro}). *J Biomol Struct Dyn*, **40**(7): 3003-3010.
- Shivanika, C., Kumar, D., Ragunathan, V., et al. 2020. Molecular docking, validation, dynamics simulations, and pharmacokinetic prediction of natural compounds against the SARS-CoV-2 main-protease. *J Biomol Struct Dyn*, **40**(2): 585-611.
- Srivastava, A. K., Kumar, A., Tiwari, G., et al. 2020. In silico investigations on the potential inhibitors for COVID-19 protease. *arXiv Preprint*: 1-12.
- Tran, J. Q., Gerber, J. G., & Kerr, B. M. 2001. Delavirdine. *Clin Pharmacokinet*, **40**(3): 207-226.
- Trott, O., & Olson, A. J. 2010. AutoDock Vina: improving the speed and accuracy of docking with a new scoring function, efficient optimization, and multithreading. *J Comput Chem*, **31**(2): 455-461.
- Wan, Y., Shang, J., Graham, R., et al. 2020. Receptor recognition by the novel coronavirus from Wuhan: an analysis based on decade-long structural studies of SARS coronavirus. *J Virol*, **94**(7).
- Ye, Z.-W., Yuan, S., Yuen, K.-S., et al. 2020. Zoonotic origins of human coronaviruses. *Int J Biol Sci*, **16**(10): 1686.
- Zaki, A. M., Van Boheemen, S., Bestebroer, T. M., et al. 2012. Isolation of a novel coronavirus from a man with pneumonia in Saudi Arabia. *N Engl J Med*, **367**(19): 1814-1820.
- Zhang, H., Penninger, J. M., Li, Y., et al. 2020. Angiotensin-converting enzyme 2 (ACE2) as a SARS-CoV-2 receptor: molecular mechanisms and potential therapeutic target. *Intensive Care Med*, **46**(4): 586-590.
- Zhou, P., Yang, X.-L., Wang, X.-G., et al. 2020. A pneumonia outbreak associated with a new coronavirus of probable bat origin. *Nature*, **579**(7798): 270-273.
- Zimmermann, P., & Curtis, N. 2020. Coronavirus Infections in Children Including COVID-19 - An Overview of the Epidemiology, Clinical Features, Diagnosis, Treatment and Prevention Options in Children. *The Pediatric Infectious Disease Journal*, **39**(5): 355-368.
- Zu, Z. Y., Jiang, M. D., Xu, P. P., et al. 2020. Coronavirus disease 2019 (COVID-19): a perspective from China. *Radiology*, **296**(2): E15-E25.

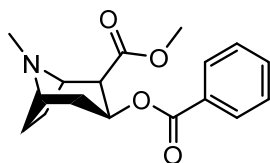
SUPPLEMENTARY INFORMATION

Table S1. Chemical structures of chloroquine, hydroxychloroquine and the 74 antiviral compounds which were utilised for the virtual screening against SARS-CoV-2 Mpro.

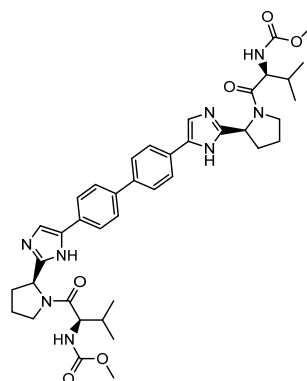
			
Chloroquine	Hydroxychloroquine	Abacavir	Acyclovir
			
Adefovir	Amantadine	Amprenavir	Arbidol
			
Atazanavir	Baloxavir marboxil	Boceprevir	Cidofovir



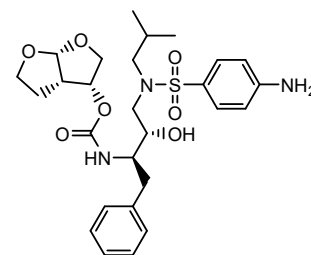
Cobicistat



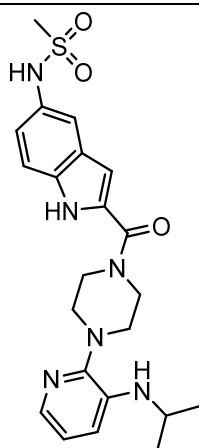
Cocaine



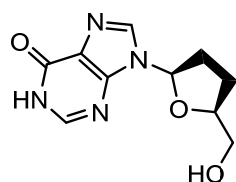
Daclatasvir



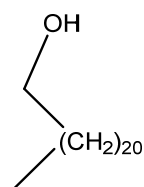
Darunavir



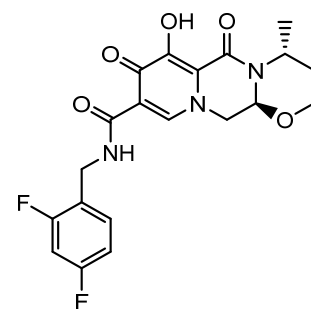
Delavirdine



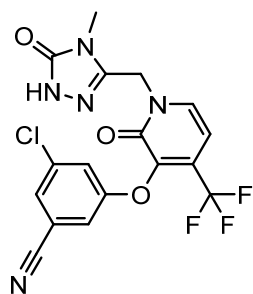
Didanosine



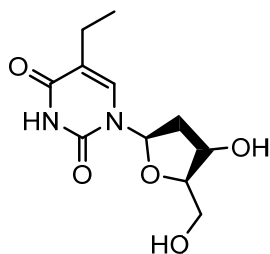
Docosanol



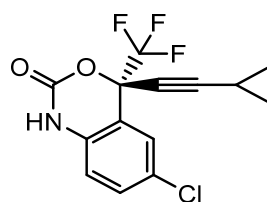
Dolutegravir



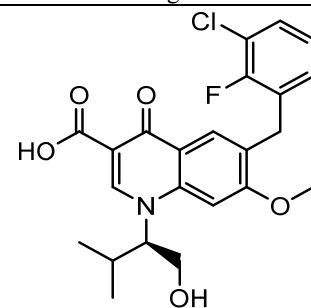
Doravirine



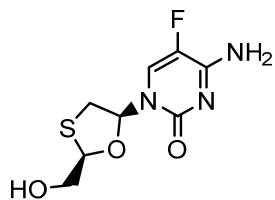
Edoxudine



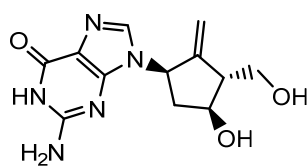
Efavirenz



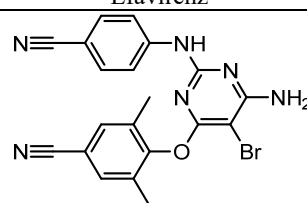
Elvitegravir



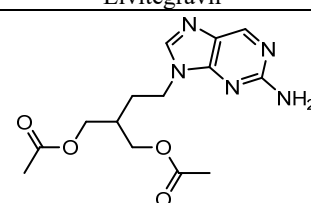
Emtricitabine



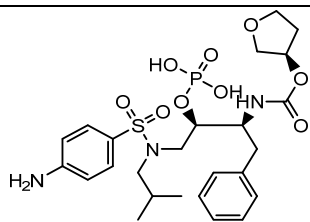
Entecavir



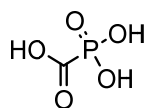
Etravirine



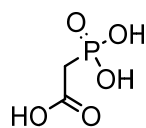
Famciclovir



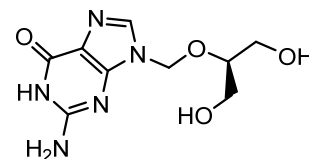
Fosamprenavir



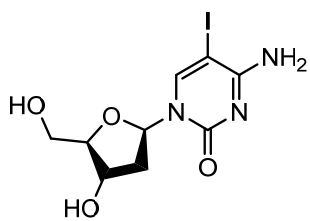
Foscarnet



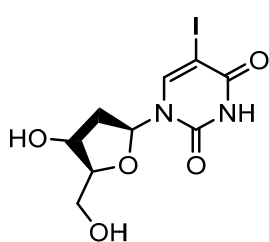
Fosfonet



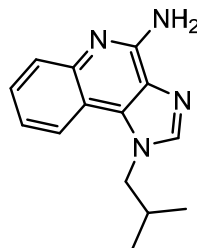
Ganciclovir



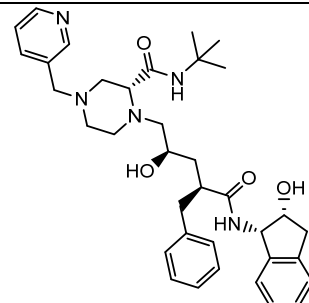
Ibacitabine



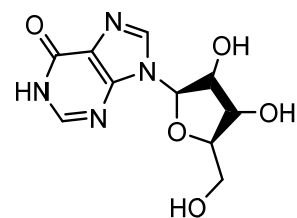
Idoxuridine



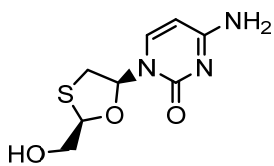
Imiquimod



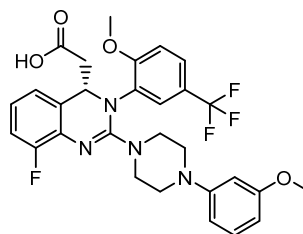
Indinavir



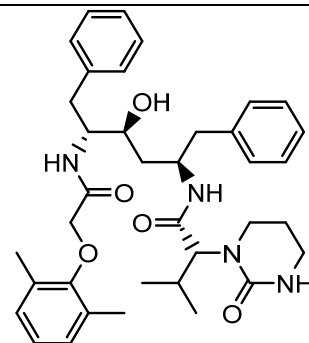
Inosine



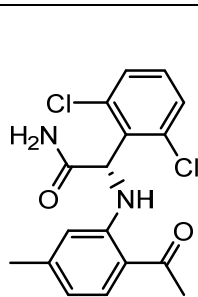
Lamivudine



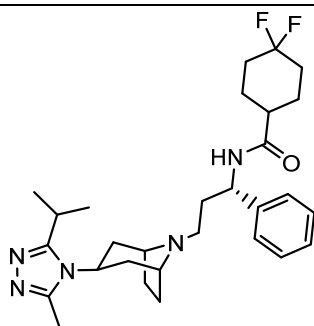
Letemovir



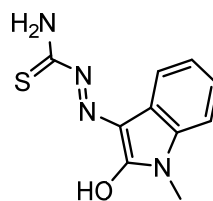
Lopinavir



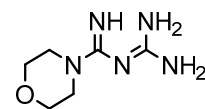
Loviride



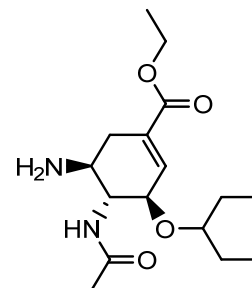
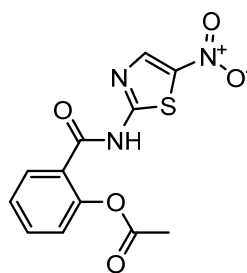
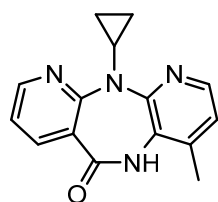
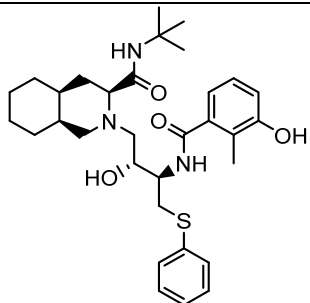
Maraviroc

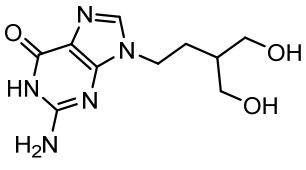
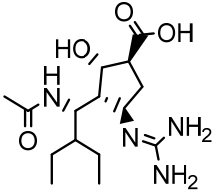
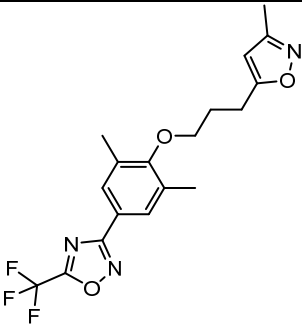
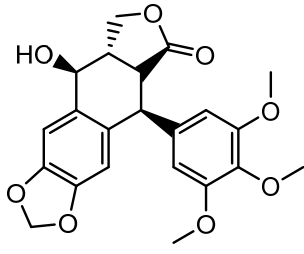
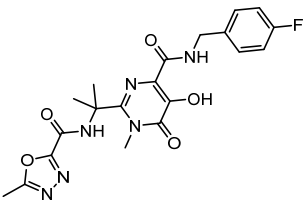
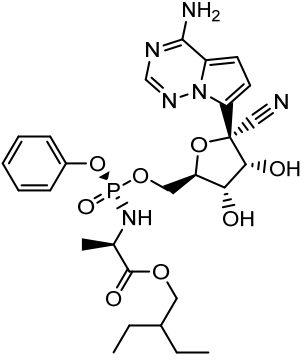
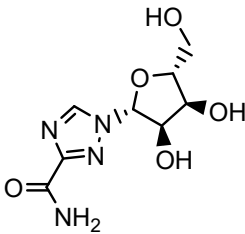
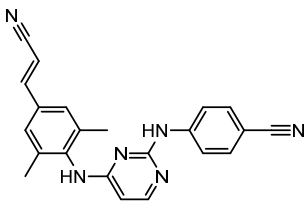
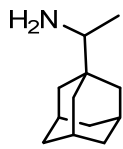
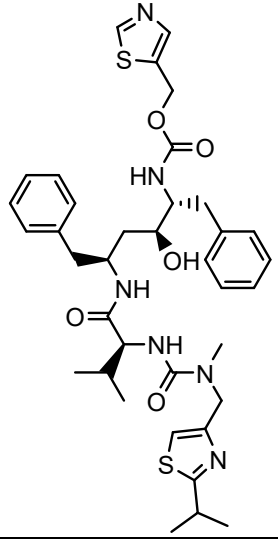
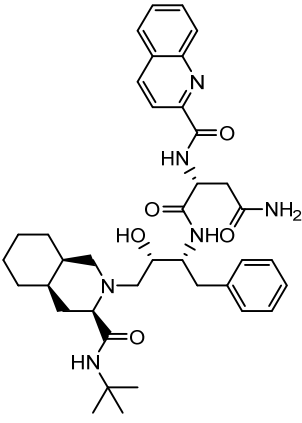
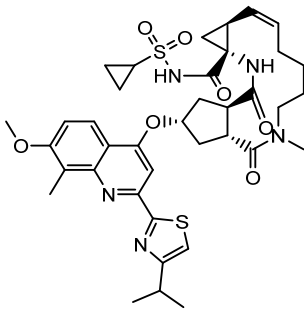
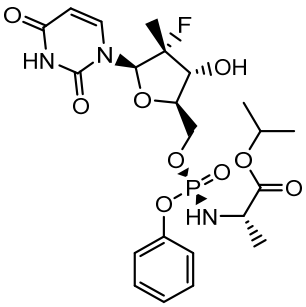
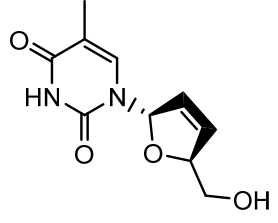
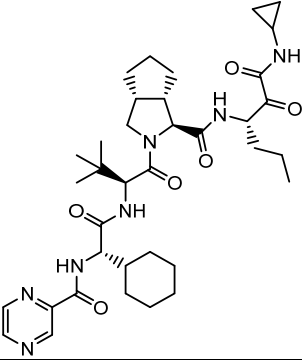
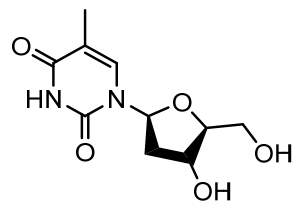


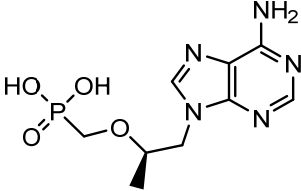
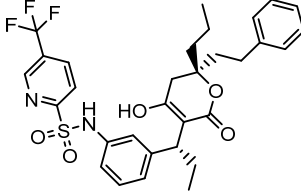
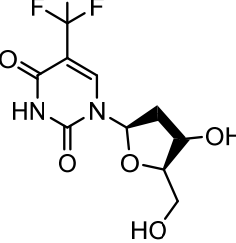
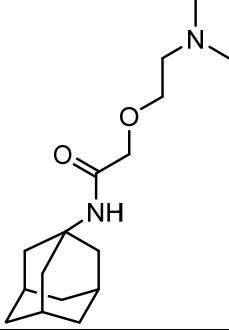
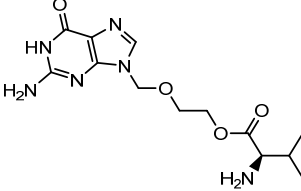
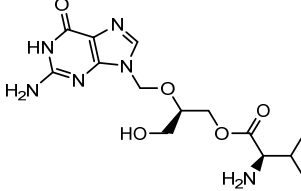
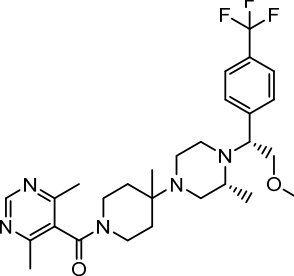
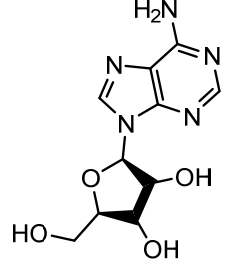
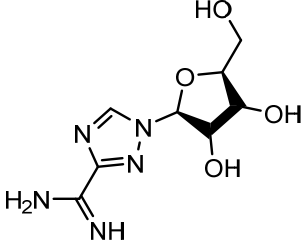
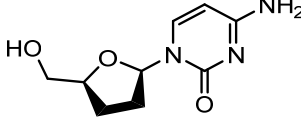
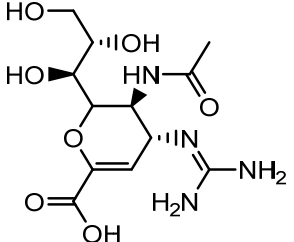
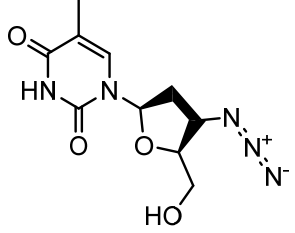
Methisazone



Moroxydine



Nelfinavir	Nevirapine	Nitazoxanide	Oseltamivir
			
Penciclovir	Peramivir	Pleconaril	Podophyllotoxin
			
Raltegravir	Remdesivir	Ribavirin	Rilpivirine
			
Rimantadine	Ritonavir	Saquinavir	Simeprevir
			

Sofosbuvir	Stavudine	Telaprevir	Telvivudine
			
Tenofovir	Tipranavir	Trifluridine	Tromantadine
			
Valaciclovir	Valganciclovir	Veciviroc	Vidarabine
			
Viramidine	Zalcitabine	Zanamivir	Zidovudine

